Renewable Energy 162 (2020) 489–503

Contents lists available at ScienceDirect

Renewable Energy

journal homepage: www.elsevier.com/locate/renene

Performance estimation of a mini-passive solar still *via* machine learning

Hisham A. Maddah [a, *], M. Bassyouni [b, c], M.H. Abdel-Aziz [a, d], M. Sh Zoromba [a, e], A.F. Al-Hossainy [f, g]

[a] Department of Chemical Engineering, King Abdulaziz University, Rabigh, 21911, Saudi Arabia
[b] Department of Chemical Engineering, Faculty of Engineering, Port Said University, 42526, Egypt
[c] Materials Science Program, University of Science and Technology, Zewail City of Science and Technology, Giza, 12578, Egypt
[d] Chemical Engineering Department, Faculty of Engineering, Alexandria University, Alexandria, Egypt
[e] Chemistry Department, Faculty of Science, Port Said University, 42521, Port Said, Egypt
[f] Chemistry Department, Faculty of Science, Northern Border University, Arar, 1321, Saudi Arabia
[g] Chemistry Department, Faculty of Science, New Valley University, 72511, Al-Wadi Al-Gadid, Al-Kharga, Egypt

ARTICLE INFO

Article history:
Received 18 April 2020
Received in revised form
31 July 2020
Accepted 3 August 2020
Available online 13 August 2020

Keywords:
Water distillation
PS insulation
Single-slope
Machine learning
Mini solar still

ABSTRACT

Achieving high water productivity in single-basin solar stills remains a challenge and may require efficient still insulation and downscaling to ease experimentation. Here, mini-passive polystyrene (PS)-based single-slope solar still is designed for brackish water desalination. Supervised machine learning regressions are applied to create trained models from experimental results. The proposed method aims to develop accurate predictive models *via* dimensional analysis and datasets expansion from in-between randomization. Built models predicted the still performance (η) when replacing PS with another wall-insulating material. We correlated the water-glass temperature (T_w–T_g) and evaporative coefficients (h_{ewg}) to the still outputs using the stepwise linear regression (SLR) showing minimum statistical errors ($R^2 \approx 1$) and RMSE<0.016. A good agreement between theoretical, numerical, and experimental results is observed; while decreasing feed rates boosts evaporation/condensation. The still achieved a maximum $\eta = 18.33\%$ corresponding to F = 30 mL/day, T_w–$T_g = 4.6\ ^\circ C$, $h_{ewg} = 21.11\ W/m^{2\circ}C$, and radiative water-glass coefficient (q_{rwg}) = 0.188 W/m^2 at 15:00 time. Hourly-measured still outputs fitted against NASA insolation followed similar patterns confirming the successful operation. Polyurethane (PU) and Silica are found to be promising wall-insulating candidates for maximizing the still output owing to their low k_{ins}. This work paves the way towards retaining the still absorbed radiation *via* thin-film foil-wrapped low-conductive insulators.

1. Introduction

Excessive production of wastewater and contamination of available freshwater sources have increasingly emerged in the last few decades due to the increasing demand for manufacturing [1,2]. Accessible Earth's freshwater sources are very limited and only account for 1% (in the form of rivers, lakes, and underground reservoirs) from the total 71% water-covered surfaces [3–5]. Membrane desalination and/or solar still water distillation are found to be promising routes to meet the high world's demand for drinking water [1,6–8]. Desalination technologies evolved based on the ancient concept of water distillation where saline water can be heated *via* thermal energy absorption, to be evaporated and then condensed on a tilted plate producing clean water. However, membrane distillations require high energy amounts for water pumping and/or evaporation making these technologies expensive for the production of freshwater [9]. In the late 19th century, various studies [10,11] discovered the use of "solar stills" as a promising and emerging water distillation technology. The advantage of solar stills is that they only utilize solar radiation as abundant, free, environmentally friendly, and easily employed thermal energy source for seawater desalination and/or industrial water purification applications [10,11].

The first conventional (passive) large basin-type solar still plant was built in 1872, in Northern Chile, with a production capacity of

* Corresponding author.
E-mail address: hmaddah@kau.edu.sa (H.A. Maddah).

https://doi.org/10.1016/j.renene.2020.08.006
0960-1481/

approximately 23 m^3/day which remained in production for around 40 years [12]. There are two common types of solar stills: (i) passive and (ii) active, which are classified according to the heating-up mechanism. In passive stills, saline water is heated up directly from absorbed solar energy by the solar basin; whereas active solar stills involve other integrated active elements (e.g. heater or boiler) that aid in raising the water temperature. Yet, passive stills are preferred over active ones owing to their conventional design and less water production costs [13]. The main components of any solar still include: (i) a water inlet at the feed-side, (ii) a basin with an absorber plate, (iii) a glass cover with a tilted angle, (iv) a sealed-transparent frame of glass, plastic, or metal, (v) a feed-distillate partition separator, and (vi) a collection outlet channel at the distillate-side [14–16].

Solar stills are typically evaluated from the maximum achievable freshwater productivity. However, the performance and productivity of a solar still depend on various critical factors including solar intensity, wind velocity, the surrounding temperature, water-glass temperatures, shallow water surface area, basin pad or absorber area, feed temperature, glass cover angle and transparency, and water level in the tank corresponding to feed flowrate in mL/day [14]. A very common problem in solar stills is that absorbed thermal energy gets lost to the surroundings from improper insulation yielding in poor still performance [17]. Earlier studies discussed in Table 1 show the ability to improve solar absorption and increase the daily distillate production of solar stills through design modification [18], insulation [19], phase change materials (PCM) [20], sun-tracking [21], and nanofluids [29]. For enhanced productivity, one can manipulate the still design parameters based on the forecasted environmental conditions (e.g. solar intensity, wind speed, weather temperature, humidity, etc.). Pillai et al. [15] discussed the differences in water productivity between sealed and unsealed systems. It was suspected that internal high pressure in sealed systems might suppress water phase-change and lower evaporation leading to lower productivity. Moreover, the surrounding's humidity impacts productivity in which dry air is preferred for developing evaporation rates. High ambient temperature increases productivity in unsealed systems and marginally decreases productivity in sealed systems [22,23].

The authors suggest that the use of passive solar still technology for household/personal needs is quite possible and can be commercialized for mini-applications. There is a great potential towards utilizing those mini-stills to efficiently produce freshwater in deserted areas [27]. A conducted study in Colombia revealed that it is possible to use solar stills for seawater desalination as a sustainable way to produce freshwater in arid environments [17]. Thus, households in deserted waterside areas in such countries like Saudi Arabia, Egypt, and Middle East territories, which are exposed to high solar radiation for most of the year, can build their own mini-passive solar stills for seawater desalination [28]. Market analysts have shown that there is a promising potential for small-scale solar systems in remote urban and agricultural areas. Introducing an efficient mini-passive household solar still system powered by renewable solar energy is critically important for household members living in water-scarce areas [27]. Nevertheless, technical and economic assessments must be conducted to check commercial feasibility of mini solar stills.

A major obstacle to overcome is heat loss, which can be addressed *via* various designs for perfect basin sealing and insulation using insulating materials on basin walls. Minimized heat escape has been previously addressed by using multi-layer insulating films [29–33] consist of wood, cotton, bubble wrap, galvanized glass, plastic, and/or other polymeric films with total film thickness ~ 30–100 mm. Khalifa et al. found out that walls and/or base insulation thickness have a significant impact on the productivity of a basin type solar still. A comparison between the results of experiments conducted on simple single-slope solar stills showed improvement in productivity (%) when using Styrofoam sheets (density = 35 kg/m^3, thermal conductivity = 0.029 W/m·°C) with a thickness of 60 mm (80%) [29]. Various theoretical and experimental studies found the still productivity to be enhanced (%) using 10–50 mm of unidentified material (40–50%) [34], 10–150 mm of wood (60%) [35], 50 mm of Styrofoam (9%) [25], and 25 mm of glass wool (2.24 L/m^2) [36]. As a rule, blackened interior surfaces maximize solar absorption while insulated exterior surfaces minimize heat losses. The still productivity (D) was previously correlated to the insulating material thickness ($\mathscr{T}$) *via*: $D = 1023\ \mathscr{T}^3 - 408.8\ \mathscr{T}^2 + 45.34\ \mathscr{T} + 1.81$ [29].

In recent work, Arunkumar et al. [31] utilized carbon impregnated foam as a porous absorber for thermal storage, with a bubble-wrap of 30 mm as inexpensive insulation in single-slope solar still ($A = 0.50\ m^2$) which increased productivity by 35% (2.3 L/m^2·day). The presence of small air pockets is ideal for achieving the lowest thermal conductivity perfect for low temperature solar thermal applications. Uninsulated stills had ~1/3 lower evaporative coefficient inside the basin as compared to solar stills with insulation, with maximum $h_{ewg} = 47.5\ W/m^2 \cdot K$ [31]. Rubber material is found to be the best basin material to improve absorption, storage, and evaporation effects [37]. Conventionally, a wooden frame with glass wool or sawdust insulation is used in simple solar stills, but such systems like this would have design issues including water leakage from the basin or distillate channel and excessive precipitation due to poor sealing [31].

According to the authors' knowledge, the minimum reported

Table 1
Recent studies conducted in conventional single-basin, double-basin, double-slope, and tubular solar stills with their reported average still output.

Study Year	Still Output (mL/day·m^2)[a]	Remarks	Ref.
2019	1506	Tubular solar collector hybrid-assisted solar still consisting of a single-stage desalination system (double-slope basin) connected to a tubular solar heater (blackened coil tube).	[19]
2018	3735	Solar still with an external solar collector and a phase change material (PCM).	[20]
2017	4000	Double-slope solar still with a solar-heating system (collectors); theoretical study.	[24]
2013	Single-basin: 2545 Double-basin: 4908	Single-basin and double-basin solar stills fabricated with a tilted glass cover at 12° and 36°, respectively, with a basin size of 0.9 m × 0.7 m × 0.008 m (volume ≈ 5040 cm^3).	[18]
2010	Passive: N/A, η = 22.7% Active: N/A, η = 38.55%	PV sun-tracking system for use as a solar collector for single-slope stills (for both passive and active solar stills).	[21]
2004	Single-basin: 2844 Double-basin: 3911	Single-basin and double-basin solar stills (with an inner surface area 90 cm × 50 cm for each still).	[25]
1994	1109	Conventional single-slope solar still.	[26]

[a] Averaged reported productivities per unit surface area of the still basin.

insulation thickness is ~20 mm [38]. It remains a challenge to create thin insulating films which can efficiently retain absorbed thermal energy. Thus, in the present work, we discuss the application of a unique/thin polymer insulating layer; the insulating layer placed on the inside glass walls consists of a polystyrene (PS) sheet (thickness = 3 mm) with Al-foil (thickness = 0.04 mm), with black-taped glass walls from the outside (thickness = 0.2 mm), giving a total insulating film (including the glass-walls) around 6 mm only. PS has a very low thermal conductivity ($k_{PS} \approx 0.033$ W/m·°C) that is approaching the poor air conductivity ($k_{air} = 0.0255$ W/m·°C). The 3 mm foil-wrapped PS-layer is an interesting combination since the PS is expected to keep absorbed thermal energy which is further promoted from light reflections (*via* aluminum foil) within the black-taped basin, increasing the water temperature rapidly. For more details regarding the still design specifications and the used materials, please refer to our earlier work [39,40].

In the present work, we designed and constructed a uniquely insulated mini-passive PS-based single-slope solar still. The 6-mm thick insulated walls consist of [black-tape, glass, PS, Al-foil] is believed to minimize the heat loss for maximum productivity. The solar still performance and distillate-water outputs were evaluated at different feed flowrates using heat transfer theoretical models and experimental results. We estimated the average water-glass convective (h_{cwg}), evaporative (h_{ewg}), and radiative (h_{rwg}) heat transfer coefficients from evaporation-condensation to be correlated with the distillate outputs. Recorded daily water productivities were studied against generated climate data (e.g. insolation, humidity, and ambient temperatures) in the March–April period. Maximum h_{ewg} values and radiative coefficients (q_{rwg}) were determined for different water amounts, then correlated with the observed heat loss from the radiative glass-to-air coefficient (q_{rga}). Hourly-recorded still outputs were attributed to hourly solar insolation to confirm the successful operation. Moreover, machine learning (ML) tools "stepwise linear regression=(SLR) learner" and datasets expansion from in-between randomization were applied to create trained models from experimental results (PS training datasets) and randomly generated input datasets correlated to outputs *via* dimensional analysis. This allowed us to accurately estimate water-glass temperature (T_w–T_g), h_{ewg}, and theoretical efficiency (or productivities) of the proposed mini-passive single-slope solar still when using different insulating materials. The possibility of improving the still performance by using low thermally conductive wall-insulating materials has been investigated using theoretical and ML models.

2. Experimental setup

A small PS-based single-slope passive solar still was initially designed and then constructed from inexpensive available market materials including (i) plexiglass sheets for frame building, (ii) water-proof and silicon sealant for the water basin, (iii) construction water-proof epoxy adhesive for connecting glass sheets, (iv) black rubber pad for thermal energy absorption, (v) aluminum foil for light reflection, (vi) PS foam sheets for still insulation from inner basin walls, (vii) black insulation duct tape for minimized energy loss from the still, and (viii) a removable cover neutral putty for keeping the cover intact. PS insulating sheets were purchased from the Goodfellow Group Co. (USA) as "transparent PS Sheet: ST313" with 3 mm thickness. Materials specifications of PS(ST313) included information about water absorption over 24 h < 0.4%, low thermal conductivity @ 23 °C of <0.1–0.13 W/m·°C, upper working temperature 50–95 °C, and thermal expansion coefficient of 30–210 × 10^{-6} K^{-1} [41]. The optimal still insulation will keep absorbed energy remain in the still accelerating the rise in water temperature. Keeping the captured energy within the still can be also maximized from selecting the right tilting angle of the glass cover. According to Raikwar [42], it is common to design passive solar stills with a single-slope inclination of either 23° or 30°, which is supposed to maximize the energy capture as well as the freshwater production rate. Kumar et al. [11] showed that the still performance at a 30° inclination increased by about 1.5% as compared to using a 23°. However, a slope angle of 20° was selected in the design of the mini-passive solar still to check the production rates in a lower angle case. The tilted top glass cover was designed to be a removable cover where the purchased neutral putty can be applied or removed for cover installation and removal, respectively. The fabricated solar still mini-basin and frame dimensions, which are scaled-down on purpose, are shown in Fig. 1, Fig. 2 and Table 2. The AutoCAD isometric 3D designs with the still principal elements and side view are illustrated in Fig. 1**(a)** and **(b)**, respectively, with dimensions in cm.

The following experimental measurement tools were used: (i) two digital thermometers: to record changes in the glass cover and water temperatures in the daytime during the study period; one thermometer was placed on the glass cover (topside) and the other one was submerged in the feedwater; (ii) a milliliter beaker: to measure the exact water volumes of both feed and distillate; and (iii) a conductivity meter: to identify and check the feed and distillate conductivities. The designed PS-insulated passive solar still is shown in Fig. 2 for both the constructed glass passive solar still without being insulated yet, Fig. 2**(a)** and **(c)**, and after being insulated with or without the neutral putty for cover installation, Fig. 2**(b)** and **(d)**.

After the construction phase of the solar still container and a successful leakage test, the solar still was placed in an open area (e.g. rooftop) in the southern region of Los Angeles, CA (34°01′13.6″N, 118°17′45.1″W). We conducted the experiments from March to April 2017 (from 9:00 a.m. to 6:00 p.m.) since the sun's radiation energy (insolation) was estimated to be close enough to the maximum levels reported for July–August as illustrated in the supplementary information (Figure S1). The impact of available solar radiation on the saline water evaporation/condensation rates was analyzed with respect to measured temperatures. The solar still was kept under insolation during March–April months to measure daily outputs. Average sun radiation of 354.67 W/m^2 was estimated from average radiation data reported by (Honsberg, 2014 [43] and NASA [44]) to relate experimental water-glass temperatures to theoretical predictions. Highly efficient solar stills are characterized by large T_w–T_g that would maximize the still productivity from enhanced water evaporation and condensation rates. Brackish water samples were prepared in our lab to resemble natural brackish water (feed) with an average conductivity of 1075 μS/cm. Water feed volumes of 30, 60, 80, and 120 mL were chosen for the daily experiments under solar irradiation. Gupta et al. [1] reported that the approximate salinity of brackish water should be 0.05–3% based on present dissolved salts, which is equivalent to 1000–80,000 μS/cm [1].

Water was fed into the system before the installation of the removable glass cover. Since no feed inlet and/or tube was connected to the container, the glass cover was designed to be removable and water was fed into the feed side manually (from the top). A removable neutral putty was applied around the glass cover to close any gaps to maintain proper sealing and insulation that would prevent heat escape from the still during the experiment (radiation absorption). The water and glass temperatures were measured every hour simultaneously over the daytime by using two digital thermometers (thermocouples) with high accuracy of ± 0.1 °C. The greater the difference between glass and water temperatures, the more heat transfer was gotten; thus, higher

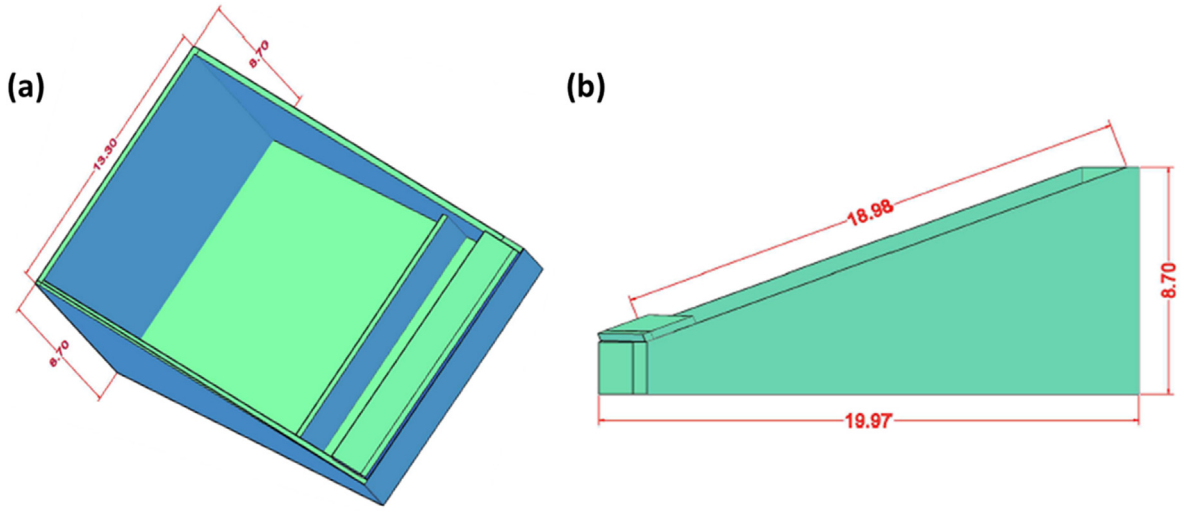

Fig. 1. The designed PS-based passive solar still: (a) The AutoCAD isometric 3D shape design showing the still principal elements as the top, bottom, slope, front, back, and partition glass slides with dimensions in cm; (b) The AutoCAD side view design with dimensions in cm.

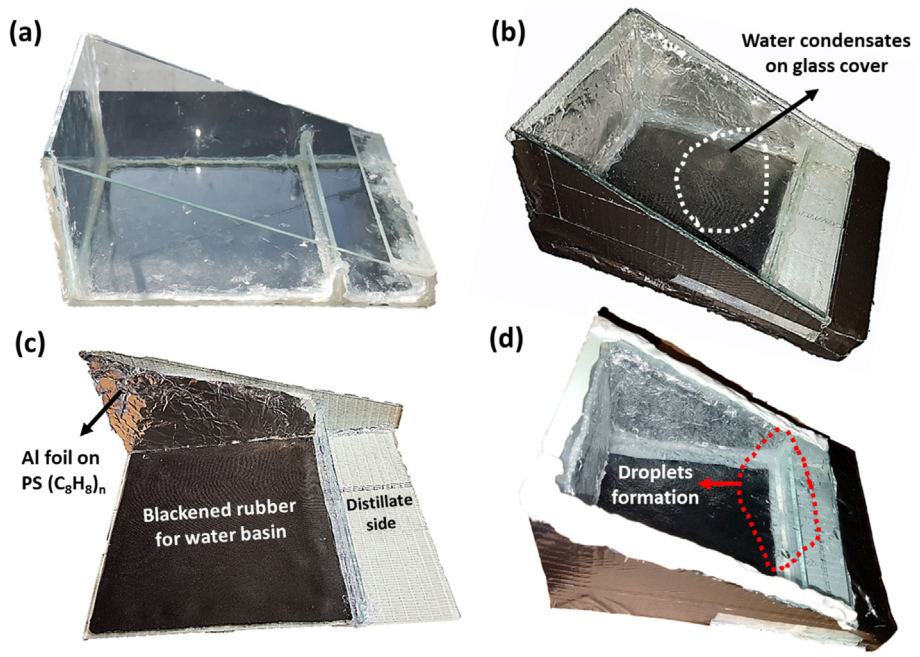

Fig. 2. The designed PS-based passive solar still: **(a)** The initial construction of the glass passive solar still before being insulated; **(b)** The final construction of the glass passive solar still after being insulated and tested for brackish water desalination showing water condensates under solar insolation; **(c)** A closer look on the bottom and side parts with the materials utilized for keeping absorbed radiation energy to increase evaporative heat transfer coefficients; **(d)** The installed glass cover with neutral putty to keep absorbed energy and build-up freshwater droplets to be collected on the distillate-side.

evaporation and condensation rates were observed. A collection beaker was placed on the distillate-side (drain) to collect and measure the purified water volume in milliliters (mL); thus, it would be possible to calculate the still performance for the different feed samples from their corresponding flowrates.

Using a worldwide climate data generator from the NASA database *via* "ArcGIS Online World Geocoding Service" [44], we generated ambient temperature (T_{air}), insolation, and relative humidity (RH = ∅) of the surrounding, from the known coordination, for 61 days (March–April 2017), Fig. 3**(a)**. Variations in T_{air} and ∅ were observed with an inverse relationship between both variables, where high insolation (3.65–8.33 kW-hr/m^2) is believed to increase temperatures and lower humidity. Four days 7, 19, 43, and 47 datasets for 30, 60, 80, and 120 mL/day samples, respectively, (from March–April) were taken for further analysis and performance comparisons. These days are identified in the study range area at the temperature-humidity intersections in Fig. 3**(a)**. The selection of the four days was made to have reliable comparisons of the still performance when using different flowrates under the impact of almost similar atmospheric conditions T_{air} = 12–15 °C, RH = 52–62%, and average wind speed = 4.4 m/s. The effect of both RH and T_{air} on water productivity can be prominent as shown in Fig. 3**(b)**; thus, it is inevitably important to consider days with similar ambient conditions for understanding the impact of feed

Table 2
Assigned dimensions of the different glass parts utilized in the construction phase.

Part Location	Quantity	Dimension[a]
Topside (cover)[b]	1	12.7 × 17.78 cm (5″ by 7″)
Bottom side	1	12.7 × 17.78 cm (5″ by 7″)
Slope sides[c]	2	Length: 19.37 cm (7.6″); IR: 8.7 cm (3.5″); AR: 2 cm (0.78″)
Frontside (low rise)	1	12.7 × 2 cm (5″ by 0.78″)
Backside (high rise)	1	12.7 × 8.7 cm (5″ by 3.5″)
Partitions	2	12.7 × 2 cm (5″ by 0.78″)

[a] Glass thickness of 3 mm is not considered.
[b] Sealant rubber is added to the glass cover to close any gaps.
[c] There is 1 cm bottom-distillate-side-gap filled with sealant; IR: Initial rise; AR: Angle rise.

flowrates on the still output.

3. Mathematical equations and methods

Basic solar sill models and heat transfer equations were previously derived from the general heat balance equation, which have been used in our investigations to determine the required solar still parameters, including the partial pressures of the glass (P_g) and the water (P_w) sides from Eq. (1) and Eq. (2), respectively [11,14,17,45–49].

$$P_g = exp\left[25.317 - \frac{5144}{T_g}\right] \quad (1)$$

$$P_w = exp\left[25.317 - \frac{5144}{T_w}\right] \quad (2)$$

Since water and glass temperatures are known and can be measured during the experimental work, it is easy to proceed in our calculations for the water-side and the glass-side partial pressures. Therefore, we can calculate the associated heat transfer coefficients and determine their impact on the still performance/output. The convective (h_{cwg}) and evaporative (h_{ewg}) heat transfer coefficients from water-to-glass (within the still) are defined in Eq. (3) and Eq. (5), respectively, which are calculated from experimentally recorded temperatures and their corresponding partial pressures. Moreover, the water-to-glass heat transfer rate (q_{ewg}) is explicitly dependent on h_{cwg} and can be determined from Eq. (4). Nonetheless, h_{ewg} is the most important and critical parameter when it comes to the still design; this is because evaporative coefficients are attributed to water evaporation and condensation rates that should be maintained high enough for maximum still performance and freshwater production [11,14,17,45–49].

$$h_{cwg} = 0.884 \times \left[(T_w - T_g) + \left\{\frac{(P_w - P_g)}{268900 - P_w}\right\} \times T_w\right]^{1/3} \quad (3)$$

$$q_{ewg} = 16.273 \times 10^{-3}\, h_{cwg}\, (P_w - P_g) \quad (4)$$

$$h_{ewg} = \frac{16.273 \times 10^{-3} \times h_{cwg}\, (P_w - P_g)}{T_w - T_g} \quad (5)$$

Radiative heat transfer coefficient (h_{rwg}) from water-to-glass is calculated from Eq. (6) and effective emissivity ($\in_{eff}$) from Eq. (7). It is noticed that the radiative coefficient strongly depends on both water and glass temperatures that are affected by solar radiation. High solar irradiation increases the difference between water and glass temperature which yields larger h_{rwg}. The emissivity ($\in$) of both water and glass also plays a key role in the calculations of h_{rwg} [11,14,17,45–49].

$$h_{rwg} = \in_{eff} \sigma \left(T_w^2 + T_g^2\right) \times (T_w + T_g) \quad (6)$$

$$\in_{eff} = \frac{1}{\left[\frac{1}{\in_g} + \frac{1}{\in_w} - 1\right]} \quad (7)$$

Total heat transfer coefficient from water-to-glass (h_{wg}) is simply the summation of the three calculated heat transfer coefficients which are associated with convection, evaporation, and radiation heat transfer modes as shown in Eq. (8) [11,14,17,45–49].

$$h_{wg} = \sum_{i=1}^{3} h_{wg} = h_{cwg} + h_{ewg} + h_{rwg} \quad (8)$$

The overall solar still efficiency (η) can be determined experimentally and/or theoretically. Experimental and theoretical efficiencies should be close enough to confirm the results of the laboratory work, which can be calculated from Eq. (9) and Eq. (10), respectively [11,14,17,45–49]. Glass and water emissivities as well as the considered feed water values and average daily solar radiation (I) are presented in Table 3.

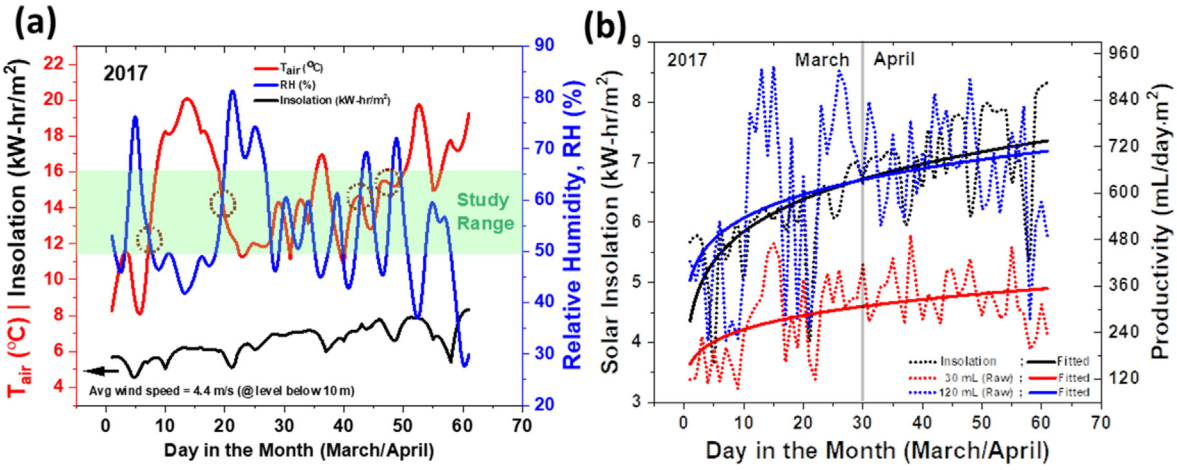

Fig. 3. Generated climate data and their impact on the accumulated still output: **(a)** Insolation, ambient temperature (T_{air}), and relative humidity (RH = ∅) during the experiment period; **(b)** Recorded daily water productivity of the still and their respective daily-averaged solar insolation.

$$\eta_{exp} = \frac{D}{F} \times 100 \tag{9}$$

$$\eta_{th} = \frac{h_{ewg}\ (T_w - T_g)}{I_r} \times 100 \tag{10}$$

Dunkle [46] suggested that the radiative heat transfer from water-to-glass (q_{rwg}) can be expressed by Eq. (11), where the heat loss by radiation from the cover to the atmosphere (q_{rga}) is given by Eq. (12); knowing that Stefan-Boltzmann constant (σ) is approximately 5.67 × 10^{-8} W/$m^2 \cdot K^4$. Sky temperature (T_{sky}) varies with amounts of both water vapor (relative humidity) and dust in the atmosphere where T_{sky} increases with humidity and dust because of the enhanced air absorption for the reflected heat from the ground. Yellot [50] and Clark and Berhal [51] proposed model, Eq. (13), can be used to estimate T_{sky} from the dew point temperature of the ambient air (t_{dp}) given by Eq. (14) that is dependent on the relative humidity (RH = ∅) of the atmosphere. The heat loss (q_{loss}) from the insulation and the overall heat transfer coefficient (U_{ins}) from Fourier's conduction can be calculated from Eq. (15) and Eq. (16), respectively [52].

$$q_{rwg} = 0.9\sigma \left(T_w^4 - T_g^4\right) \tag{11}$$

$$q_{rga} = 0.9\sigma \left(T_g^2 - T_{sky}^4\right) \tag{12}$$

$$T_{sky} = T_{air} \left[0.74 + 0.006 t_{dp}\right]^{0.25} \tag{13}$$

$$t_{dp} = f(\varnothing, T_{air}) = \frac{\left[237.3\left(\ln\varnothing + \frac{17.27T_{air}}{T_{air}+237.3}\right)\right]}{\left[17.27 - \ln\varnothing + \frac{17.27T_{air}}{T_{air}+237.3}\right]} \tag{14}$$

$$q_{loss} = U_{ins}\ (T_{ins} - T_{air}) \tag{15}$$

$$U_{ins} = \left[\frac{L_{ins}}{k_{ins}} + \frac{1}{h_{ins}}\right]^{-1} \tag{16}$$

4. Machine learning models

According to the literature, Mashaly et al. [55] utilized an artificial neural network (ANN) approach for the prediction of passive solar still productivity showing the possibility of constructing a generalized model [55]. Mathioulakis et al. [56] and Voropoulos et al. [57] further developed a simplified theoretical model capable of predicting long-term water production. Random forest (RF) and ANN non-linear ML techniques were previously applied to tubular solar still [58] to accurately predict hourly production closer to true experimental observations [58]. An earlier study utilized both linear and Gaussian regressions to develop prediction models for solar radiation (10-fold cross-validation) based on a one-year meteorological data; Gaussian models were found to have the least MSE providing a high prediction performance [59]. Altan et al. modeled a three-axis gimbal system for unmanned aerial vehicles to propose algorithms that can exactly track the target while maintaining stability [60]. Moreover, RF nonlinear methods were utilized to create a solar radiation model using five specified parameters. The high-performance recognition model identified the most important features that would impact solar radiation through a forward selection approach [61]. However, forecasting the potential productivities of different designed solar stills using built-in and pre-existing ML toolboxes remains a challenge due to the many parameters that need to be considered in models training.

Herein, the proposed method aims to develop an accurate predictive model based on supervised ML regression tools (MATLAB) and datasets expansion from in-between randomization. We took advantage of the inevitable errors in the measured and independent input values of the studied variables from our experimental results. Randomly generated input datasets in the approximated boundaries are correlated to outputs *via* dimensional analysis and proposed system equations. This allowed us to create trained models that would accurately predict productivities in a single-slope solar still. Built models were employed to marginally predict the still performance when replacing PS with another insulator with high and/or low thermal conductivities. We have also correlated T_w–T_g and h_{ewg} to the still outputs when using various wall-insulating materials in the SLR model that showed the minimum statistical errors. The estimation of the still performance when using different insulating materials have been studied *via* a supervised ML analysis [62–65]. The SLR learner toolbox in MATLAB [65] was utilized to establish the trained models from PS training datasets (inputs/outputs obtained from experiments). Investigated input data include (i) thermal conductivity (k_{ins}), (ii) feed flowrate (F), (iii) water depth (H_w) in the feed-basin, (iv) water surface area (A_s), and (v) daily solar radiation (I). Meanwhile, studied output variables involved (i) water-glass temperature difference (T_w–T_g), (ii) evaporative heat-transfer coefficient (h_{ewg}), (iii) theoretical efficiency (η_{th}), and (iv) distillate or distilled water (D). Polyurethane (PU), polyester (PE), silica aerogel (Silica), wool felt (Wool), fiberglass (FG), and peat are the studied insulating materials chosen for predicting the still performance when these insulators are incorporated instead of PS.

It is worth mentioning that we have carried out the ML analysis using inputs for an average flowrate (F = 30 ± 2 mL/day) corresponding to water depth (H_w = 1.8 ± 0.01 mm), water surface area (A_s = 0.01613 ± 0.0001 m^2), and maximum daily radiation (I = 5.32 ~ 5.34 kW-hr/m^2) with the estimated minimum/maximum k_{ins} for the selected insulators as shown in Fig. 4**(a)** according to the literature [66–68]. The intended output values were taken for PS from the experiments as [T_w–T_g = 4.58 ± 0.02 °C, maximum h_{ewg} = 12.745 ± 0.475 W/$m^2 \cdot$°C, η_{th} = 16.4 ± 0.52%, and D = 4.93 ± 0.48 mL] in order to build the PS training datasets and ML models.

Trained models were used in predicting the still performance when replacing PS with another insulting material in our designed system. Once PS training models are determined, we utilized the same SLR code to the future datasets obtained for the chosen insulating materials. Future datasets had the same inputs as in PS

Table 3
Feedwater, radiation, and other solar still related parameters with their taken values in the experimental, theoretical, and machine learning calculations.

Variable/Parameter (Symbol)	Unit	Value [Ref.]
Feed flowrate (F)	mL/day	30, 60, 80 and 120
Average daily solar radiation (I)[a]	kW-hr/m^2	5.32 [43,44]
Radiation time (t)	hr	9:00 to 18:00; or 9 h
Rate of incident solar energy (I_r)[b]	W/m^2	354.67
Water surface area (A_s)	m^2	0.01613
Stefan Boltzmann constant (σ)	kg s^{-3} K^{-4}	5.67 × 10^{-8} [53]
Glass emissivity ($\in_g$)	–	≈0.86 [48,54]
Water emissivity ($\in_w$)	–	≈0.95 [48,54]

[a] The average solar radiation was determined from the average radiations of months March–April in 2017 [43,44].
[b] Estimated from daily radiation since the study was conducted for 9 h only (daytime).

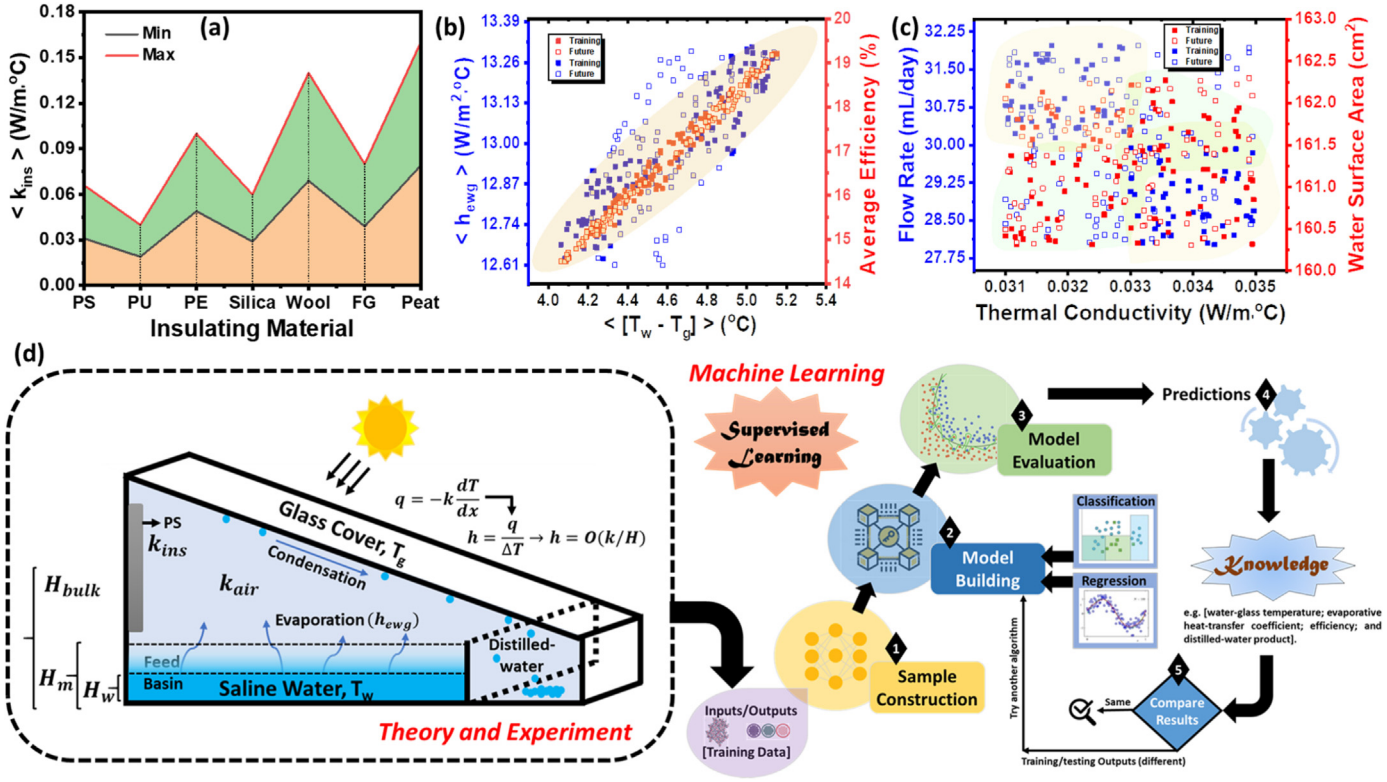

Fig. 4. Supervised machine learning (ML) data utilized in the PS training/future analysis with ~30 mL/day flowrate: **(a)** Thermal conductivities of various studied insulating materials; **(b)** Output datasets determined for PS training/future relating water-glass temperature-difference to both water evaporative coefficient and still efficiency from input datasets; **(c)** Input datasets for the PS training/future model calculations; **(d)** Schematic showing the heat transfer mechanism and other system parameters utilized in the ML analysis and theoretical modeling, theory and experiment results are taken as inputs for building training datasets from the PS-based solar still, the machine learning algorithm using "stepwise linear regression=(SLR) learner" for prediction of still performance when using different insulating materials.

training datasets with k_{ins} as the only different variable to predict future results (outputs). The generated datasets (training/future) consist of five matrices of [100 × 1] for each of the 7 studied insulators according to the previously selected inputs. This is also equivalent to saying that we have generated a one [100 × 5] matrix for each of the 7 studied insulating materials to relate k_{ins} to h_{ewg}, T_w–T_g, and water productivity (total of 7 matrices of [100 × 5]). Training datasets were generated using PS-based solar still experimental results and each variable (input/output) determined from using the "Random-Between" function in EXCEL for the previously given input ranges. In other words, only PS output was produced to carry out the ML analysis for the other insulators and estimate their outputs. Future datasets were randomly generated using the approximated boundaries for the obtained intended output values. Prediction results were obtained from four different PS-based trained models, each for one output variable, applied to the randomly generated input [100 × 5] of the different insulating materials. Thermal conductivity is a material property which was utilized as a leading input parameter with different boundary limits (max/min) based on the literature values and as illustrated in Fig. 4**(a)**.

Input parameters were taken independently from each other whereas studied output parameters considered explicitly or implicitly dependent on insulators' thermal conductivity and other inputs. Dimensionality analysis allowed us to estimate that $(T_w - T_g) \approx \gamma \overline{H_w} \left(\frac{I_r}{k_{ins}}\right) \times \left(0.75 \frac{H_m}{H_w}\right) \times \left(\frac{F}{A_s}\right)$, where the introduced temperature-difference coefficient (γ) found to be $\gamma \approx 0.06$ for our system, $\overline{H_w} = [H_w|_{F=30} / H_w|_{F<30}]$, F in mL/day, and the maximum h_{ewg} was estimated from the proposed correlation $h_{ewg} = \left[\frac{k_{ins}+k_{air}}{H_{bulk}-H_w}\right] \times 0.7 \left(\frac{k_{ref}}{k_{ins}}\right)$ based on the well-known Fourier-law for the heat flux ($q = -k[dT/dx]$) and ($h = q/dT$) [69–71]. This gives us the estimated order-of-magnitude $(O)h \sim (O)[k/H]$ in agreement with our proposed equations, where k_{air} = 0.0255 W/m·°C [72], $k_{ref} = k_{PS} = 0.033 \pm 0.002$ W/m·°C, $H_{bulk} = 5$ cm in bulk-air near to the glass-cover; η_{th} from Eq. (10); D from Eq. (9) with the assumption $\eta_{th} = \eta_{exp}$. Theoretical analysis and obtained equations were carried out using dimensionality and from comparisons with our experimental results. The steps used in the development of the ML regression models are presented in the flowchart in Fig. 5; which starts with datasets curation used in training/testing regressions for estimating the passive solar still performance with various insulating materials.

PU has the lowest thermal conductivity among the other studied materials indicating its potential in preventing solar energy escape from the solar still. High thermal conductivity yields in loss of absorbed energy (heat from the sun) to the surrounding; which would result in the poor still performance for water distillation. The PS training/future datasets were obtained from both inputs [Fig. 4**(c)**] and outputs [Fig. 4**(b)**] from experimental results and dimensionally derived equations. Randomly generated PS inputs resulted in almost similar outputs where training/future (T_w–T_g vs. h_{ewg} and/or η) data collapsed. Collapsible output PS-datasets confirms the validity of the equations in relating input parameters to output results. The heat transfer mechanism in single-slope passive solar still is illustrated in Fig. 4**(d)** with identified H, k, and T parameters and the basic equations for the derivation method of the proposed h_{ewg} correlation from the dimensionality analysis. The

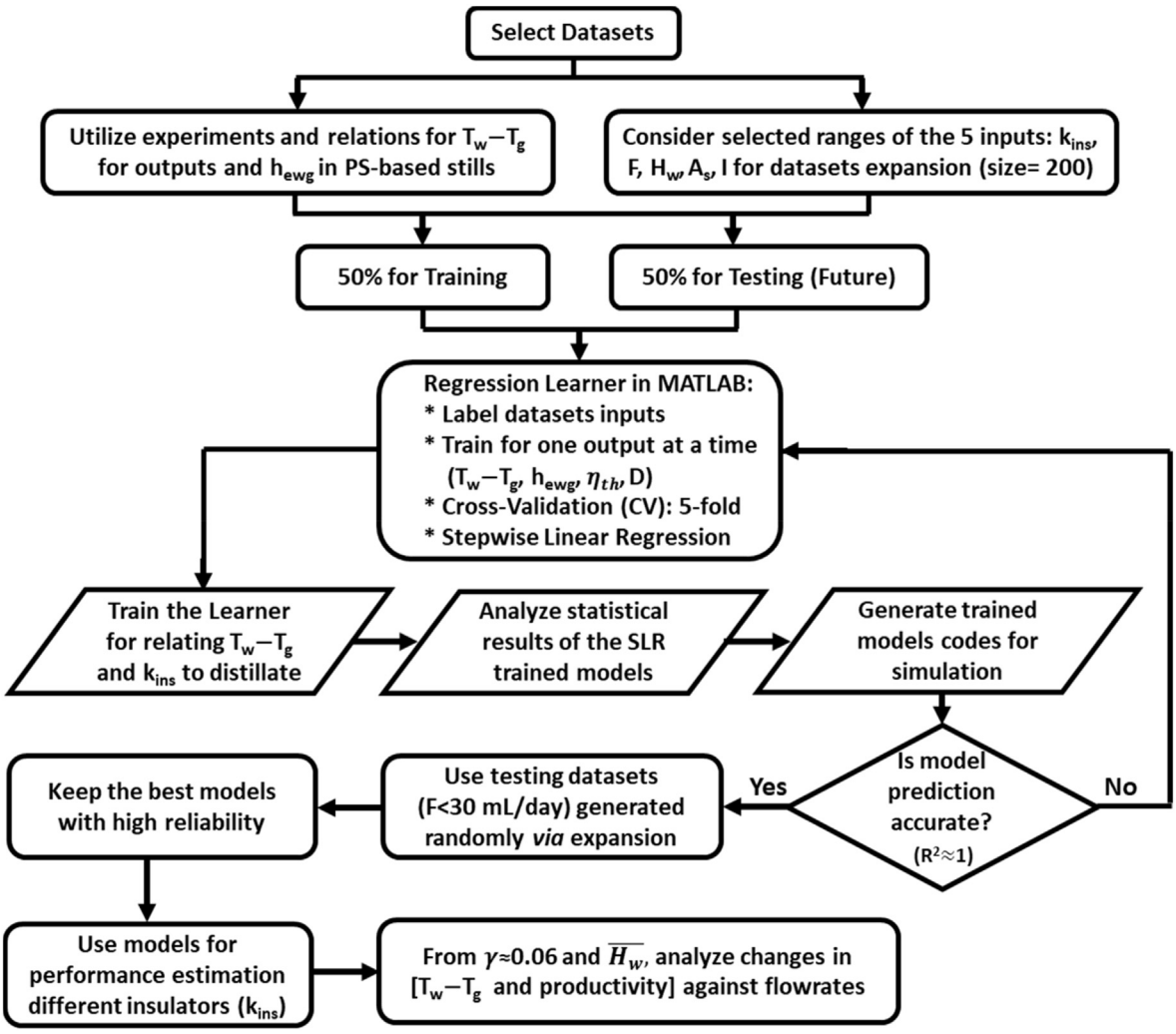

Fig. 5. Flowchart describing the steps used in the development of the supervised machine learning (ML) models: Starting from datasets curation used in training/testing regressions for code generation, which are then utilized in estimating the still performance with various insulating materials.

supervised ML algorithm is shown in Fig. 4**(d)** where training datasets were built from the experimental results of PS-based solar still. Built models were able to predict the still performance when using different insulating materials for F≤30 mL/day. Note that $\left(0.75\frac{H_m}{H_w}\right)$ and $0.7\left(\frac{k_{ref}}{k_{ins}}\right)$ terms serve as correction factors in the proposed equations since (i) T_w-T_g decreases with higher flux rates $\left(\frac{F}{A_s}\right)$, and (ii) h_{ewg} increases with low k_{ins}, but the correction factor terms are required for the correctness of our dimensionality analysis.

5. Mechanism of heat transfer for water evaporation

The mechanism of heat transfer and solar radiation absorption inside the solar still is illustrated in Fig. 4(d) and can be simplified as the following: (i) transmitted solar radiation goes through the glass cover and mostly gets absorbed by the blackened-bottom surface (collector; or basin liner) in the feed basin, (ii) from the basin liner increased temperature, saline water heats up and its temperature will rise more than that of the still air and/or the cover where T_w-T_g initiates evaporation, (iii) water vapor density of humid air increases from continuous evaporation and released latent heat leading to condensation at the inner surface of the cover, (iv) condensed water droplets trickle down the tilted cover, due to gravity force, to the distillate-water side for collection *via* a trough [10,73,74]. The former mechanism is valid for single-slope passive solar still. The heat transfer mechanisms of other several complex designs (spherical, pyramidal, double basin, and hemispherical, etc.) can be found elsewhere [10,23,74,75].

Water evaporation may take place at low temperatures, but the rate of evaporation/condensation can be significantly accelerated at higher temperatures reaching the dew point for vapor condensation (when the temperature inside the still is much higher than the ambient temperature). Ideally, it is desired to have a very high T_w and very low T_g to promote h_{ewg} due to high-temperature gradient, influencing evaporation/condensation and water productivity [15]. The use of a solar-collector heat-exchanger system has been suggested in earlier works to rapidly increase T_w and boost condensation [76,77]. The side-walls of solar stills are often made of insulating/impermeable materials to keep the absorbed solar radiation for raising the water temperature. It remains a challenge to create thin insulating films that can efficiently retain absorbed thermal energy. Thus, we focused on applying a very thin PS layer (thickness = 3 mm) with aluminum foil (thickness = 0.04 mm). PS has a very low thermal conductivity (k_{PS} = 0.033 W/m·°C) that is

approaching the poor air conductivity ($k_{air} = 0.0255$ W/m·°C). The 3-mm foil-wrapped PS-layer is an interesting combination since the PS keeps absorbed thermal energy which is further promoted by light reflections within the black-taped basin, increasing the water temperature rapidly. The roles of the specified basin insulation components in promoting the heat transfer mechanism are (i) basin blackened rubber liner increases solar radiation absorption to the water promoting T_w–T_g, (ii) aluminum foil applied on the inner surface of the side-walls (top of PS) reflects sunlight radiations inside the container; hence, developing evaporation/condensation rates from the increased T_w, (iii) inner-wall PS foam sheets (in the inner side surfaces of the still basin) further induce the still insulation by keeping absorbed thermal energy that is maintained from the possible reduction in both q_{rga} and h_{cwg}, and (iv) outer-wall black insulation duct tapes covering the still side-walls minimize heat loss and radiation energy escape of the absorbed solar energy due to the non-reflection mechanism.

6. Results and discussion

The changes in water and glass cover temperatures have been observed over the daytime (under solar radiation) for the different studied feed flowrates (30, 60, 80, and 120 mL/day) as shown in Fig. 6**(a)-(d)**, respectively. It was implied that lower feed flowrates are preferable to promote maximum achievable temperature and T_w–T_g which would enhance h_{ewg} for better performance and evaporation rate.

Similarly, decreasing water feed quantities resulted in boosting h_{ewg} and h_{rwg} in the solar still, as calculated for 30, 60, 80, and 120 mL/day in Fig. 7**(a)-(d)**, respectively. The 30 mL/day feed flowrate achieved the highest evaporation rates with a maximum evaporative coefficient of $h_{ewg} = 21.11$ W/m^2·°C at t = 15, (i.e. 3:00 p.m.). This might be achieved due to the reduced heat capacity (J/°C) of water which is an extensive property that scales down with low water volume.

The determined heat transfer coefficient average values for the passive PS-insulated single-slope solar still are shown in Fig. 8**(a)**, with a comparison between different feed flowrates. When daily feed rates decreased, h_{rwg} coefficients had slightly increased with prominent progression in the h_{ewg} coefficient. This can explain the high evaporation rates observed at low flowrates. We found good agreement between the theoretical and experimental results illustrated in Fig. 8**(b)**, confirming the model validity to predict the still performance. Theoretical efficiencies should always be larger than their corresponding experimental efficiencies (for the same flowrate), which was as expected. However, the 30 mL/day feed scenario showed a maximum experimental efficiency that is slightly greater than the maximum theoretical efficiency. This could explain the possibility of reaching the maximum theoretical limit (ideal case) in mini-solar stills with low flowrates due to the highest achieved h_{ewg}. The relationship between T_w–T_g (at noon times: t = 15) and the observed performance has been plotted in Fig. 8**(c)** which showed a good linear fit indicating that high-temperature differences would boost evaporation/condensation rates and increase the still productivity for freshwater. Evaporative heat transfer coefficients have been also correlated to the still efficiency in Fig. 8**(d)** showing that high h_{ewg} rates are necessary and may only happen when there are noticeable temperature differences. We have related the feed water flowrates (feed quantities) to the still productivity and the number of stages required to treat 50% of the inlet as shown in Fig. 8**(e)** and (f), respectively. Both productivity and treatment stages (required days to treat 50% of the feed) are found to proportionally increase with feed flowrates. Maximum water productivity of ~446 mL/day·m^2 was observed for 120 mL/day flowrate (this is during day 47, where day 60 showed a productivity of ~720 mL/day·m^2 in Fig. 3**(b)**), with nine stages required to have >60 mL of freshwater. This shows the promise in using mini solar stills to treat >50% of inlet saline water volume in almost a week with fixed daily rates.

Fig. 3**(b)** relates solar insolation to the still productivity over the

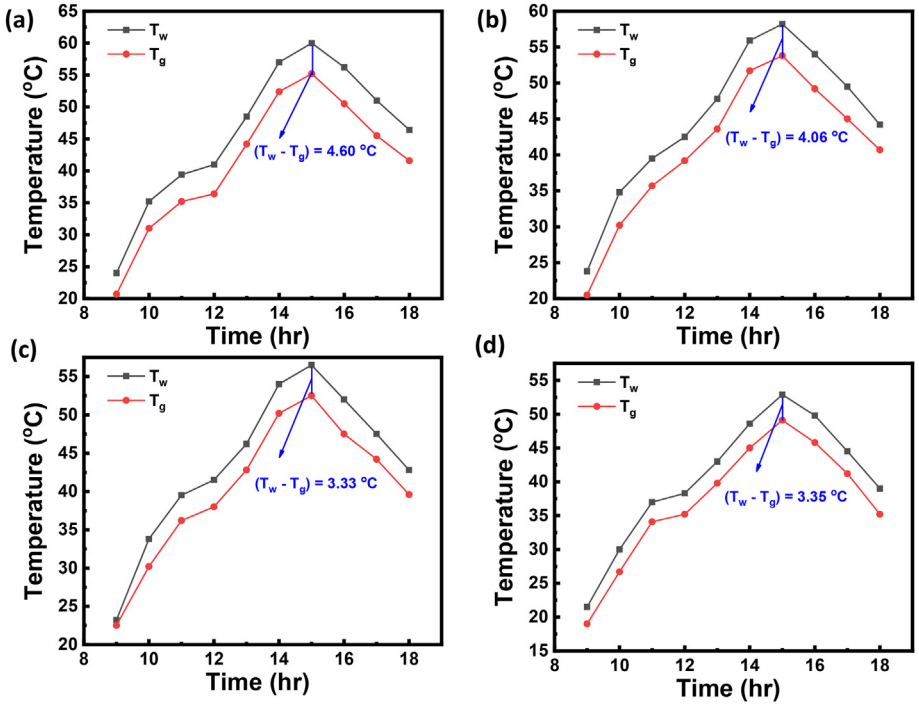

Fig. 6. Measured solar still water and glass temperatures with the observed water-glass temperature difference (T_w–T_g) driving the evaporation/condensation rates in the different studied feed flowrates: **(a)** 30 mL/day; **(b)** 60 mL/day; **(c)** 80 mL/day; **(d)** 120 mL/day.

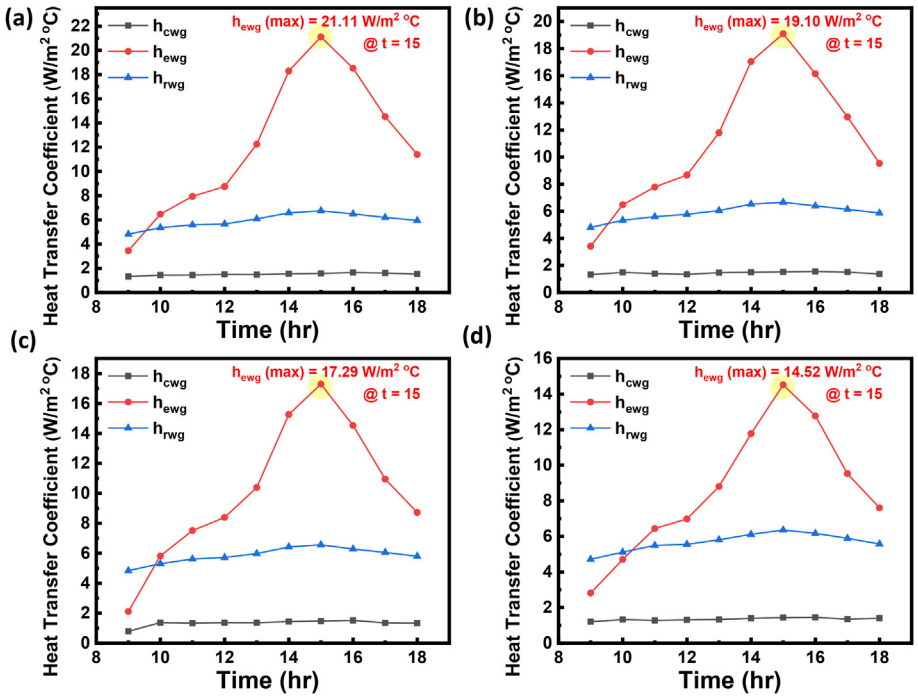

Fig. 7. Convective (h_{cwg}), evaporative (h_{ewg}), and radiative (h_{rwg}) heat transfer coefficients observed from water evaporative/condensation rates in the designed passive PS-based solar still under solar radiation (~354.67 W/m^2) for the different feed flowrates: **(a)** 30 mL/day; **(b)** 60 mL/day; **(c)** 80 mL/day; **(d)** 120 mL/day. Evaporative heat transfer coefficients decreased with water volume and reported values here are at t = 15 (i.e. 3:00 p.m. local time).

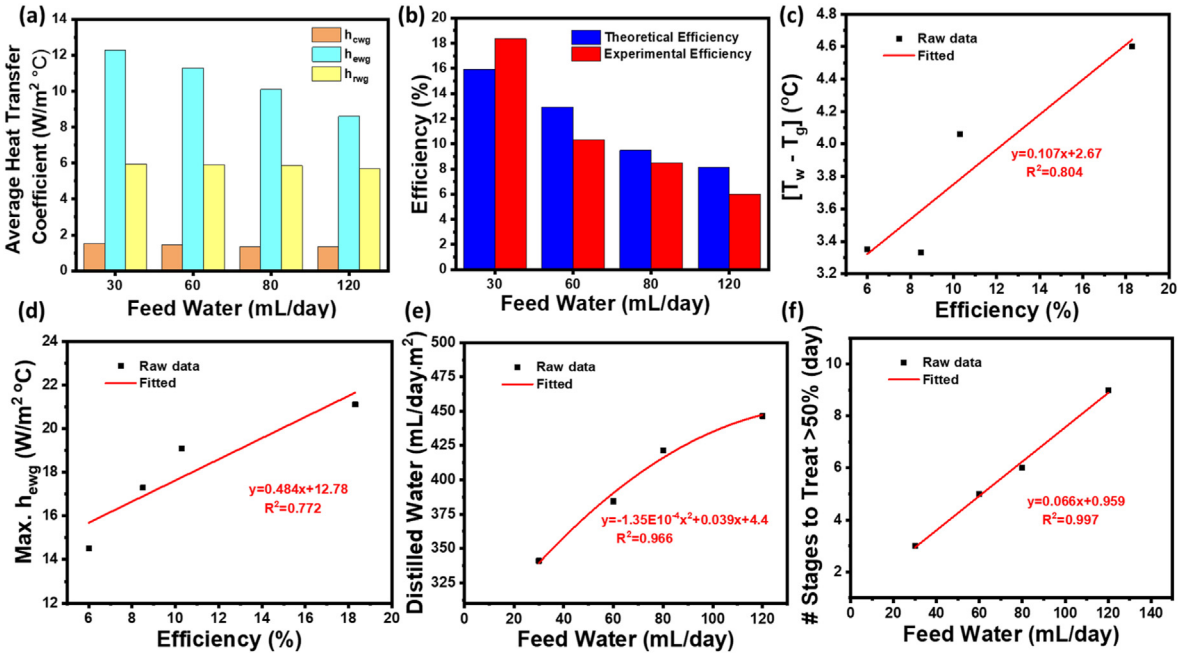

Fig. 8. Heat transfer coefficients and water-glass temperatures with their relationship to the feed flowrate (mL/day) and still performance or water productivity: **(a)** Averaged convective, evaporative, and radiative heat transfer coefficients for the different feed flowrates; **(b)** Theoretical and experimental solar still efficiencies at different feed rates; **(c)** Water-glass temperature difference and its relationship with the observed performance; **(d)** Maximum evaporative heat transfer coefficients correlated with the passive still efficiency; **(e)** Second-order polynomial increase in distilled water quantity with increasing water flowrates; **(f)** Required number of stages or days for the treatment of >50% of different feed flowrates. Note that **(c)** and **(d)** are determined at the maximum absorption hours: t = 15 (i.e. 3:00 p.m. local time).

two-month study period for the 30 mL/day and 120 mL/day feed rates. It was evident that productivities increase with solar radiation following the same insolation pattern. Average recorded productivities found to be ~263 and ~536 mL/day·m^2 for the feed rates 30 and 120 mL/day, respectively. Thus, larger water amounts yield in higher productivity, but with lower still performance attributed to the slight decreases in h_{ewg}.

Trained SLR models estimated the still output (as a function of

T_{air}) when using different wall-insulating materials with similar PS thickness, Fig. 9**(a)** and **(b)**. The results predicted that PU and Silica are the optimal insulating materials to maximize the still output for the flowrates 30 mL/day and 120 mL/day, respectively. The trained models did not show PU as the optimal expected insulator for the high flowrates ~120 mL/day since training datasets were taken from the 30 mL/day experiments. Interestingly, low thermally conductive insulators (e.g. Silica) did not contribute much in accelerating the still output for the 120 mL/day scenario. This might be explained by the relatively large water volume increasing thermal energy requirements. A minimum of 4-fold increase in energy requirements show that we need much higher h_{ewg} for a maximum efficiency ~20.6% (i.e. 10% efficiency for the 120 mL/day using Silica may be improved to 20% if $T_{air} = 40^{\circ}$C based on the extrapolation of the curve in Fig. 9**(b)**).

Water productivities from the PS-based solar still confirmed the theoretical model reliability since results were in agreement with Fig. 8**(b)** and **(c)** with a marginal error of ~10%. Absorbed and lost radiation energies were correlated to the radiative coefficients q_{rwg} and q_{rga}, respectively, as shown in Fig. 9**(c)**. Low water amounts developed q_{rwg} over the daytime with a maximum $q_{rwg} = 0.188$ W/m^2 at 15:00 time. The high q_{rwg} for 30 mL/day is attributed to the minimized loss of solar radiation from the still (low q_{rga}, note that q_{rga} is in negative since thermal energy is lost). Conversely, adding more water in the feed hinders q_{rwg} indicating poor radiative heat transfer, low-temperature difference, and reduced still output. Hourly-measured still outputs for day 7 and day 47 for 30 mL/day and 120 mL/day, respectively, were plotted and fitted (Gaussian fit in ORIGIN) against the recorded insolation obtained from NASA datasets, Fig. 9**(d)**. The patterns of insolation and still outputs are almost identical explaining the successful design and operation of the novel mini-passive thin-film PS-insulated solar still. The accumulated still outputs from Fig. 9**(d)** are equivalent to the daily productivities reported in Fig. 8**(e)** since both are obtained from the PS-based solar still experiments.

Trained SLR models predicted the still output and distillation performance when replacing PS wall-insulating material with selected insulators as shown in Fig. 10**(a)** and **(b)**. The models showed a high coefficient of determination ($R^2 \approx 1$) and RMSE<0.016. The high predictions accuracy was confirmed from the estimated PS-based still performance found close enough to our experimental results. To further assess the accuracy and performance of the prediction models, the authors have checked for the trained models statistical errors. It seems that we achieved the highest $R^2 = 1$, with very low statistical errors MAE, MSE, and RMSE as shown in Table 4 and obtained from the ML analysis figures presented in the supplementary information (Figures S2-S11). This is a result of the proposed in-between randomization method to expand the training samples to 100 points before the training step. Training and testing analysis showed the models capability of predicting future performance and productivities based on the 50% testing datasets from experiments. The codes of the four developed models *via* the SLR learner are reported in the supplementary information (section 2) based on the five specified inputs.

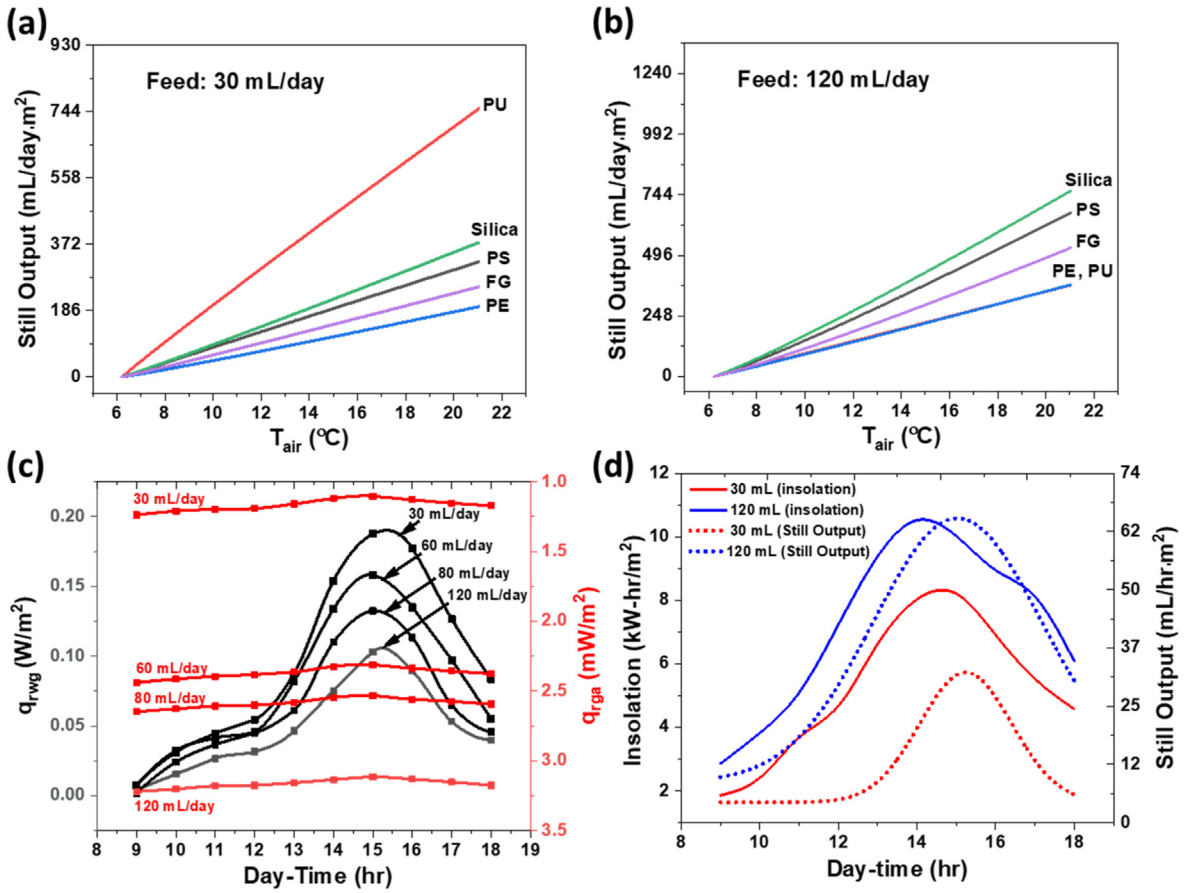

Fig. 9. **(a)** Estimated still output when using different insulators with 30 mL/day feed; **(b)** Estimated still output when using different insulators with 120 mL/day feed; **(c)** Radiative water-to-glass coefficient (q_{rwg}) and heat loss from radiative glass-to-air coefficient (q_{rga}) for different water amounts; **(d)** Hourly-recorded still outputs attributed to hourly solar insolation for day 7 (30 mL/day) and day 47 (120 mL/day).

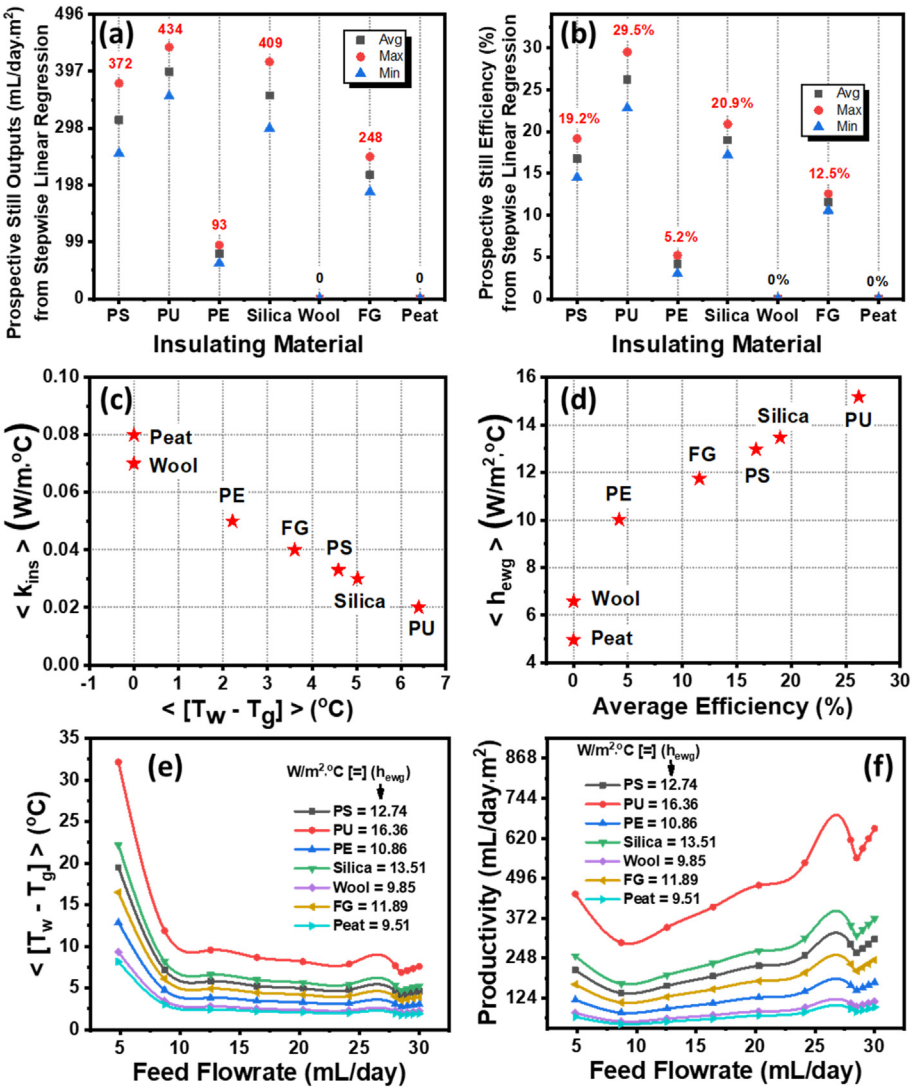

Fig. 10. Stepwise linear regression (SLR) machine learning analysis combined with the theoretical equations for studying the use of different insulating materials in the designed mini-passive single-slope solar still: **(a)** Estimated max/min and averaged still productivity; **(b)** Predicted max/min and averaged still efficiency; **(c)** Water-glass temperature difference correlated to the insulator thermal conductivity; **(d)** Evaporative heat transfer coefficient related to the improved still performance; Correlated feed flowrates to **(e)** temperature differences; and **(f)** productivity carried out while h_{ewg} (W/m^2·°C), inset, is held constant determined from our dimensional analysis calculations.

Table 4
Statistical errors obtained from the various applied SLR trained regression models for the prediction of the solar still efficiency, h_{ewg}, productivity, or T_w–T_g [a]

Statistical Error	Efficiency (η)	h_{ewg}	Productivity (D)	T_w–T_g
RMSE	0.0167	0.0033	0.0070	0.0025
R^2	1.00	1.00	1.00	1.00
MSE	2×10^{-4}	1.1×10^{-5}	4.9×10^{-5}	6.4×10^{-6}
MAE	0.0126	0.0025	0.0053	0.0018

[a] SLR=Stepwise-Linear-Regression with Cross-Validation (CV): 5-fold; Reliable models are considered with $R^2 > 0.90$ that show the minimum MSE or RMSE; Abbreviations: the coefficient of determination (R^2), the mean square error (MSE), the root mean square error (RMSE), and the mean absolute error (MAE).

The basin liners and the other still variables were kept the same in the calculation steps to identify the impact of insulation on the still productivity. PU and Silica showed the possibility of having a very high still performance (~20–30%) with maximum still outputs of 434 and 409 mL/day·m^2, respectively (Fig. 10**(a)**). This is indicative that high productivities are achievable with low thermally conductive insulators wrapped with foil papers to reflect solar light and keep absorbed energy inside the still. Water-glass temperature differences are found to increase with the decrease in k_{ins}, Fig. 10**(c)**, while the still efficiency is proportionally related to h_{ewg} resulted from such insulation, Fig. 10**(d)**. Correlated feed flowrates to both T_w–T_g and still productivity for the different insulators are shown in Fig. 10**(e)** and **(f)**, respectively. The enhanced still outputs for PU and Silica for the 30 mL/day flowrate (620 and 366 mL/day·m^2, respectively) is feasible because the material's poor thermal conductivity accelerates evaporation/condensation rates. However, the trained model seems to be invalid for F≤5 with a good approximation for 5<F < 29 (F in mL/day) since training datasets were gathered from experiments with F = 30 mL/day.

Still productivities (normalized to the water surface area) have been compared with literature and earlier studies on single-basin solar stills. The still outputs were in the range 360~720 mL/day·m^2, which is approximately one-order-of-magnitude less than the reported single-slope literature productivities (e.g. 4300 mL/day·m^2 [20], 3911 mL/day·m^2 [25], and 2595 mL/day·m^2 [18]). The lower water productivity rates of the designed mini solar still were

associated with the available still volume. Since the PS-stills were scaled down in size by 15-fold (322.6 cm^3), as compared to other conventional still sizes with a maximum volume of 5040 cm^3 [18], the mini-basin solar still achieved decent outputs of ~446 mL/day·m^2. Thus, if one is capable of scaling-up our system volume by 15-fold while keeping the same design specifications, the authors believe that a production rate up to 5115~6690 mL/day·m^2 is achievable and is high enough to outnumber most of the current literature results on single-basin solar stills. This could be possible because PS insulation and blackened still walls/basin play a key role in improving the performance by keeping the absorbed solar energy, decreasing heat loss, and improving solar absorption.

The below remarks summarize the discussed results and main findings:

- Lower feed flowrates are preferable to promote T_w-T_g and h_{ewg} boosting evaporation and water productivity due to the reduced heat capacity (J/°C) of water.
- Theoretical models show good accuracy for the prediction of the still performance.
- High-temperature differences boost evaporation/condensation rates and increase productivity.
- PU and Silica are predicted as the optimal wall-insulating materials to maximize the still output ~446 mL/day·m^2) with high still performance (~20–30%).
- Low water amounts develop q_{rwg} attributed to the minimized loss of solar radiation (low q_{rga}).
- Insolation and hourly still outputs should follow the same patterns for successful design and operation.
- High productivities are achievable with low thermally conductive insulators wrapped with foil papers.
- Trained models showed high $R^2 \approx 1$ and low RMSE<0.016, achieving high prediction accuracy.
- High rates of evaporation occur with an enhanced evaporative coefficient (h_{ewg}), increased water-glass radiative coefficient (q_{rwg}), and reduced radiation losses (q_{rga}).
- Scaling-up the volume by 15-fold for the designed novel mini-passive thin-film PS-insulated solar still could result in production rates up to 5115~6690 mL/day·m^2.

7. Conclusion

We demonstrated the performance evaluation of designed mini-passive polystyrene (PS)-insulated single-slope solar still for the treatment of brackish water. The experimental work is conducted in Los Angeles (34°01′13.6″N, 118°17′45.1″W) during March–April 2017. Heat transfer coefficients are estimated from theoretical and numerical models based on the experimental results to predict the still maximum productivity. Decreasing feed rates is found to linearly promote evaporation/condensation rates due to the observed increases in T_w-T_g, where the evaporative heat transfer coefficient (h_{ewg}) noticeably increased at 30 mL/day. Also, low water amounts developed q_{rwg} that reached 0.188 W/m^2 at 15:00 time from the minimized loss of solar radiation. The 6-mm thick insulated walls consist of [black-tape, glass, PS, Al-foil] are believed to minimize the heat loss for maximum productivity. The PS-insulated still achieved maximum $\eta = 18.33\%$ which corresponds to $T_w-T_g = 4.6$ °C and $h_{ewg} = 21.11$ W/m^2 °C at noon times. Both productivity and treatment stages are found to proportionally increase with feed flowrates. The maximum productivity of ~720 mL/day·m^2 is observed with a flowrate of 120 mL/day. Regardless of the feed flowrates, the increase in T_w-T_g and/or h_{ewg} is found to drastically improve the still performance. Hourly-measured still outputs fitted against the reported NASA insolation followed almost identical patterns explaining the successful design and operation.

Dimensional analysis and datasets expansion *via* in-between randomization from the experimental results (PS training datasets) allowed us to develop accurate predictive models using the stepwise linear regression (SLR) supervised machine learners. Five specified parameters including insulators' thermal conductivity (k_{ins}) are studied and correlated to T_w-T_g, h_{ewg}, and efficiency. Created trained models estimated the water-glass temperature, h_{ewg}, and theoretical efficiency (or productivities) when replacing PS with another wall-insulator. The proposed models showed a high prediction accuracy with minimum statistical errors ($R^2 \approx 1$) and RMSE<0.016 for F≤30 mL/day. PU and Silica are found to be the optimal insulating materials to maximize the still output and achieve high performance (~20–30%) owing to their low k_{ins} that develops water-glass temperatures. The use of Al-foil integrated with such wall-insulators for a black-taped basin can keep absorbed solar energy within the still due to the reduced wall thermal conductivity and the promoted light reflections. However, designing efficient still insulation remains a challenge and future studies may require the application of multiple insulating layers integrated with light-reflecting layers and light-absorbing nanoparticles. This work opens a new avenue towards further downscaling solar stills to ease experimentation, considering that excess heat loss needs to be yet investigated in future works *via* creating a unified machine learning model. Early and future experiments should be utilized to build such models that would include the impact of design modification, insulation, operating/weather conditions, sun-tracking, and nanofluids on the still performance.

CRediT authorship contribution statement

Hisham A. Maddah: Conceptualization, Data curation, Formal analysis, Funding acquisition, Investigation, Methodology, Project administration, Resources, Software, Supervision, Validation, Visualization, Writing - original draft, Writing - review & editing. **M. Bassyouni:** Writing - review & editing. **M.H. Abdel-Aziz:** Writing - review & editing. **M. Sh Zoromba:** Writing - review & editing. **A.F. Al-Hossainy:** Writing - review & editing.

Declaration of competing interest

The authors declare that they have no known competing financial interests or personal relationships that could have appeared to influence the work reported in this paper.

Acknowledgments

HAM would like to acknowledge the Saudi Arabian Cultural Mission (SACM) and King Abdulaziz University (KAU) for their support and funding.

Appendix A. Supplementary data

Supplementary data related to this article can be found at https://doi.org/10.1016/j.renene.2020.08.006.

Nomenclature

η	Solar still efficiency, %
D	Distillate flowrate, mL/day
F	Feed flowrate, mL/day
Q	Daily output, L
A_s	Area of the water surface in the solar still, m^2
I	Average daily solar radiation, MJ/m^2

q	Radiative transfer coefficient or rate of heat/energy transfer, W/m^2
h	Heat transfer coefficient, W/m^2·K
T	Average temperature, K
P	Vapor pressure, N/m^2
t	Time, h
$\in$	Emissivity, %
t_{dp}	Dew point temperature of the ambient air, K
$\varnothing$	Humidity, %
U	Overall heat transfer coefficient, W/m^2·K
L	Length, m
γ	Temperature-difference coefficient, %
H	Height, m
k	Thermal conductivity, m

Subscripts

exp	Experimental
th	Theoretical
w	Water
m	Maximum
g	Glass
r	Radiation
wg	Water-to-glass
eff	Effective
cwg	Convective heat transfer from water-to-glass
ewg	Evaporative heat transfer from water-to-glass
rwg	Radiative heat transfer from water-to-glass
rga	Radiative heat transfer from glass-to-air
sky	Ambient condition far from the ground
air	Ambient condition close to the ground <2 m
loss	Lost radiation energy to the atmosphere
ins	Insulator
ref	Reference insulator (PS)
bulk	Bulk region in the still near to glass cover

References

[1] H. Maddah, A. Chogle, Biofouling in reverse osmosis: phenomena, monitoring, controlling and remediation, Appl. Water Sci. 7 (2016) 2637–2651, https://doi.org/10.1007/s13201-016-0493-1.

[2] H.A. Maddah, Optimal operating conditions in designing photocatalytic reactor for removal of phenol from wastewater, ARPN J. Eng. Appl. Sci. 11 (2016) 1799–1802.

[3] B. Gupta, T. Kumar Mandraha, P. Edla, M. Pandya, Thermal modeling and efficiency of solar water distillation: a review, Am. J. Eng. Res. 2 (12) (2013) 203–213.

[4] H.A. Maddah, Modeling the relation between carbon dioxide emissions and sea level rise for the determination of future (2100) sea level, Am. J. Environ. Eng. 6 (2016) 52–61.

[5] G.N. Tiwari, H.N. Singh, R. Tripathi, Present status of solar distillation, Sol. Energy (2003), https://doi.org/10.1016/j.solener.2003.07.005.

[6] H.A. Maddah, A.M. Chogle, Applicability of low pressure membranes for wastewater treatment with cost study analyses, Membr. Water Treat. 6 (2015) 477–488, https://doi.org/10.12989/mwt.2015.6.6.477.

[7] H.A. Maddah, Application of finite Fourier transform and similarity approach in a binary system of the diffusion of water in a polymer, J. Mater. Sci. Chem. Eng. 4 (2016) 20.

[8] H.A. Maddah, A.S. Alzhrani, A.M. Almalki, M. Bassyouni, M.H. Abdel-Aziz, M. Zoromba, M.A. Shihon, Determination of the treatment efficiency of different commercial membrane modules for the treatment of groundwater, J. Mater. Environ. Sci. 8 (2017) 2006–2012.

[9] K. Sampathkumar, T.V. Arjunan, P. Pitchandi, P. Senthilkumar, Active solar distillation-A detailed review, Renew. Sustain. Energy Rev. (2010), https://doi.org/10.1016/j.rser.2010.01.023.

[10] T. Arunkumar, K. Vinothkumar, A. Ahsan, R. Jayaprakash, S. Kumar, Experimental study on various solar still designs, ISRN Renew. Energy. (2012), https://doi.org/10.5402/2012/569381.

[11] D. Kumar, P. Himanshu, Z. Ahmad, Performance analysis of single slope solar still, Int. J. Mech. Robot. Res. 3 (3) (2013) 66–72.

[12] N. Arellano Escudero, La planta solar de desalación de agua de Las Salinas (1872), Lit. y Mem. Una Exp. Pioner. XII (2011) 229–251.

[13] M.N.I. Sarkar, A.I. Sifat, S.M.S. Reza, M.S. Sadique, A review of optimum parameter values of a passive solar still and a design for southern Bangladesh, Renewables Wind. Water, Sol. (2017), https://doi.org/10.1186/s40807-017-0038-8.

[14] P. Kalita, A. Dewan, S. Borah, A review on recent developments in solar distillation units, Sadhana - Acad. Proc. Eng. Sci. (2016), https://doi.org/10.1007/s12046-015-0445-8.

[15] R. Pillai, A.T. Libin, M. Mani, Study into solar-still performance under sealed and unsealed conditions, Int. J. Low Carbon Technol. (2015), https://doi.org/10.1093/ijlct/ctt045.

[16] T. Libin, R. Pillai, M. Mani, Sealed-system performance of a compact stepped solar-still, Environ. Eng. Manag. J. 10 (5) (2011).

[17] A.M. Burbano, Evaluation of basin and insulating materials in solar still prototype for solar distillation plant at Kamusuchiwo community, High Guajira, Renew. Energy Power Qual. J. (2017), https://doi.org/10.24084/repqj12.395.

[18] T. Rajaseenivasan, T. Elango, K. Kalidasa Murugavel, Comparative study of double basin and single basin solar stills, Desalination (2013), https://doi.org/10.1016/j.desal.2012.09.014.

[19] O. Bait, Exergy, environ–economic and economic analyses of a tubular solar water heater assisted solar still, J. Clean. Prod. (2019), https://doi.org/10.1016/j.jclepro.2018.12.015.

[20] M. Al-harahsheh, M. Abu-Arabi, H. Mousa, Z. Alzghoul, Solar desalination using solar still enhanced by external solar collector and PCM, Appl. Therm. Eng. (2018), https://doi.org/10.1016/j.applthermaleng.2017.09.073.

[21] S.A. Mutasher, N. Mir-Nasiri, S.Y. Wong, K.C. Ngoo, L.Y. Wong, Improving a conventional greenhouse solar still using sun tracking system to increase clean water yield, Desalin. Water Treat. (2010), https://doi.org/10.5004/dwt.2010.1473.

[22] G.N. Tiwari, N.K. Dhiman, Performance study of a high temperature distillation system, Energy Convers. Manag. (1991), https://doi.org/10.1016/0196-8904(91)90133-4.

[23] M.S. Malik, M.A.S. Tiwari, G.N. Kumar, A. Sodha, Solar Distillation: a Practical Study of a Wide Range of Stills and Their Optimum Design, Construction, and Performance, Oxford Pergamon Press, 1982, pp. 11–13.

[24] O. Bait, M. Si-Ameur, Tubular solar-energy collector integration: performance enhancement of classical distillation unit, Energy (2017), https://doi.org/10.1016/j.energy.2017.09.110.

[25] A.A. Al-Karaghouli, W.E. Alnaser, Performances of single and double basin solar-stills, Appl. Energy (2004), https://doi.org/10.1016/S0306-2619(03)00005-9.

[26] V.H. Morcos, Some experimental and theoretical studies of a single basin solar still, Renew. Energy (1994), https://doi.org/10.1016/0960-1481(94)90047-7.

[27] M.T.B.F. Sales, Solar powered desalination system using Fresnel lens, IOP Conf. Ser. Mater. Sci. Eng. (2016), https://doi.org/10.1088/1757-899X/162/1/012002.

[28] F. Trieb, Concentrating Solar Power for Seawater Desalination, Stuttgart, BW, Germany, 2007.

[29] A.J.N. Khalifa, A.M. Hamood, Effect of insulation thickness on the productivity of basin type solar stills: an experimental verification under local climate, Energy Convers. Manag. (2009), https://doi.org/10.1016/j.enconman.2009.06.007.

[30] M.S.S. Abujazar, S. Fatihah, A.R. Rakmi, M.Z. Shahrom, The effects of design parameters on productivity performance of a solar still for seawater desalination: a review, Desalination (2016), https://doi.org/10.1016/j.desal.2016.02.025.

[31] T. Arunkumar, A.E. Kabeel, K. Raj, D. Denkenberger, R. Sathyamurthy, P. Ragupathy, R. Velraj, Productivity enhancement of solar still by using porous absorber with bubble-wrap insulation, J. Clean. Prod. (2018), https://doi.org/10.1016/j.jclepro.2018.05.199.

[32] B.B. Sahoo, N. Sahoo, P. Mahanta, L. Borbora, P. Kalita, U.K. Saha, Performance assessment of a solar still using blackened surface and thermocol insulation, Renew. Energy (2008), https://doi.org/10.1016/j.renene.2007.09.009.

[33] G.M. Cappelletti, An experiment with a plastic solar still, Desalination (2002), https://doi.org/10.1016/S0011-9164(02)00203-5.

[34] H.E.S. Fath, S. Elsherbiny, A. Ghazy, A naturally circulated humidifying/dehumidifying solar still with a built-in passive condenser, Desalination (2004), https://doi.org/10.1016/S0011-9164(04)00521-1.

[35] S. Aboul-Enein, A.A. El-Sebaii, E. El-Bialy, Investigation of a single-basin solar still with deep basins, Renew. Energy (1998), https://doi.org/10.1016/s0960-1481(98)00081-0.

[36] B. Jamil, N. Akhtar, Effect of specific height on the performance of a single slope solar still: an experimental study, Desalination (2017), https://doi.org/10.1016/j.desal.2017.03.036.

[37] K. Kalidasa Murugavel, K.K.S.K. Chockalingam, K. Srithar, Progresses in improving the effectiveness of the single basin passive solar still, Desalination (2008), https://doi.org/10.1016/j.desal.2007.01.062.

[38] J.C. Torchia-Núñez, M.A. Porta-Gándara, J.G. Cervantes-de Gortari, Exergy analysis of a passive solar still, Renew. Energy (2008), https://doi.org/10.1016/j.renene.2007.04.001.

[39] H.A. Maddah, Modeling and designing of a novel lab-scale passive solar still, J. Eng. Technol. Sci. (2019), https://doi.org/10.5614/j.eng.technol.sci.2019.51.3.1.

[40] H.A. Maddah, Highly efficient solar still based on polystyrene, Int. J. Innovative Technol. Explor. Eng. 8 (2019) 3423–3425.

[41] Goodfellow, Polystyrene – sheet: ST313400. http://www.goodfellow.com/catalogue/GFCat4J.php?ewd_token=CUoE0SN4GtnFriGnUVWqO9eBrbCWCG&n=GlFGV3IMKPXvEFJ7d1RW8c1F31PNJr.

[42] A. Raikwar, J. Pandey, M. Gour, Determination of total internal heat transfer coefficient of single slope solar still with different depth of water, Int. J. Emerg. Technol. Adv. Eng. 3 (2013) 2250–2459.
[43] S. Honsberg, C. Bowden, Average solar radiation. http://pveducation.org/pvcdrom/average-solar-radiation, 2014 accessed April 1, 2017.
[44] NASA, ArcGIS online world geocoding Service: prediction of worldwide energy resource. https://power.larc.nasa.gov/data-access-viewer/, 2019.
[45] O.O. Badran, M.M. Abu-Khader, Evaluating thermal performance of a single slope solar still, Heat Mass Transf. Und Stoffuebertragung. (2007), https://doi.org/10.1007/s00231-006-0180-0.
[46] R.V. Dunkle, Solar water distillation: the roof type still and a multiple effect diffusion still, Int. Dev. Heat Transf. ASME, Proc. Int. Heat Transf. Part V. 5 (1961) 895.
[47] A.S. Kumar, Y. Singh, K.P. Kuntal, Estimation of heat transfer coefficient in single slope solar still, in: Challenges Effic. Energy Technol, Clean Energy 21st Century, 2000, pp. 149–153.
[48] M. Afrand, R. Kalbasi, A. Karimipour, S. Wongwises, Experimental investigation on a thermal model for a basin solar still with an external reflector, Energies (2017), https://doi.org/10.3390/en10010018.
[49] P. Singh, J. Singh, Performance evaluation of single basin solar still, Int. J. Environ. Chem. Ecol. Geol. Geophys. Eng. 9 (2015) 1196–1199.
[50] J.I. Yellott, Passive and hybrid cooling research, Adv. Sol. Energy (1983), https://doi.org/10.1007/978-1-4684-8992-7_9.
[51] E. Clark, P. Berhal, Radiative cooling: resources and applications, in: Proc. Passiv. Work., Amherst, MA, 1980, pp. 177–212.
[52] H. Al-Hinai, M.S. Al-Nassri, B.A. Jubran, Effect of climatic, design and operational parameters on the yield of a simple solar still, Energy Convers. Manag. (2002), https://doi.org/10.1016/S0196-8904(01)00120-0.
[53] R.H. Perry, D.W. Green, Perry's Chemical Engineers' Handbook, eighth ed., 2013, https://doi.org/10.1017/CBO9781107415324.004.
[54] A. Kaushal, Varun, Solar stills: a review, Renew. Sustain. Energy Rev. (2010), https://doi.org/10.1016/j.rser.2009.05.011.
[55] A.F. Mashaly, A.A. Alazba, Neural Network Approach for Predicting Solar Still Production Using Agricultural Drainage as a Feedwater Source, Desalin. Water Treat., 2016, https://doi.org/10.1080/19443994.2016.1193770.
[56] E. Mathioulakis, K. Voropoulos, V. Belessiotis, Modeling and prediction of long-term performance of solar stills, Desalination (1999), https://doi.org/10.1016/S0011-9164(99)00030-2.
[57] K. Voropoulos, E. Mathioulakis, V. Belessiotis, Analytical simulation of energy behavior of solar stills and experimental validation, Desalination (2003), https://doi.org/10.1016/S0011-9164(02)01107-4.
[58] N. Wang, Y. Kandeal, A.W. Swidan, A. Sharshir, S.W. Abdelaziz, G.B. Halim, M.A. Yang, Prediction of tubular solar still performance by machine learning integrated with Bayesian optimization algorithm, ArXiv Prepr. 1 (2020) arXiv: 2002.03886.
[59] R. Karasu, S. Altan, A. Sarac, Z. Hacioglu, Prediction OF solar radiation based ON machine learning methods, J. Cogn. Syst. 2 (2017) 16–20.
[60] A. Altan, R. Hacıoğlu, Model predictive control of three-axis gimbal system mounted on UAV for real-time target tracking under external disturbances, Mech. Syst. Signal Process. (2020), https://doi.org/10.1016/j.ymssp.2019.106548.
[61] A. Karasu, S. Altan, Recognition model for solar radiation time series based on random forest with feature selection approach, in: IEEE 2019 11th Int. Conf. Electr. Electron. Eng, 2019, pp. 8–11.
[62] S.B. Kotsiantis, Supervised machine learning: a review of classification techniques, Inform (2007), https://doi.org/10.31449/inf.v31i3.148.
[63] Y. Baştanlar, M. Ozuysal, Introduction to Machine Learning, second ed., 2014, https://doi.org/10.1007/978-1-62703-748-8_7.
[64] O. Simeone, A brief introduction to machine learning for engineers, Found. Trends Signal Process. (2018), https://doi.org/10.1561/2000000102.
[65] Mathworks, Statistics and Machine Learning Toolbox ™ User's Guide R2017a, MatLab, 2017.
[66] Food & Agriculture Organization of the UN, Thermal insulation materials, technical characteristics and selection criteria, 1989. http://www.fao.org/3/y5013e/y5013e08.htm.
[67] Engineering ToolBox, thermal conductivity of selected materials and gases. https://www.engineeringtoolbox.com/thermal-conductivity-d_429.html.
[68] A.L. Young, H.D. Freedman, R.A. Sandin, T.R. Ford, University Physics, seventh ed., Addison-Wesley, MA, 1992. http://hyperphysics.phy-astr.gsu.edu/hbase/Tables/thrcn.html.
[69] Y.A. Cengel, A.J. Ghajar, Heat and Mass Transfer, Fundamentals & Application, fifth ed., SI Units, 2015.
[70] F.P. Incropera, D.P. DeWitt, T.L. Bergman, A.S. Lavine, Fundamentals of Heat and Mass Transfer, sixth ed., 2007, https://doi.org/10.1016/j.applthermaleng.2011.03.022.
[71] R. Byron Bird Warren, E. Stewart Edwin, N. Lightfoo, R.B. Bird, W.E. Stewart, E.N. Lightfoot, Transport Phenomena, Revised, second ed., John Wiley Sons, Inc., 2006 https://doi.org/10.1002/aic.690070245.
[72] Engineering ToolBox, Air - Thermophysical Properties, 2003.
[73] A. Ahsan, M. Imteaz, A. Rahman, B. Yusuf, T. Fukuhara, Design, fabrication and performance analysis of an improved solar still, Desalination (2012), https://doi.org/10.1016/j.desal.2012.02.013.
[74] J.C. Torchia-Núñez, J. Cervantes-de-Gortari, M.A. Porta-Gándara, Thermodynamics of a shallow solar still, Energy Power Eng. (2014), https://doi.org/10.4236/epe.2014.69022.
[75] H. Manchanda, M. Kumar, A comprehensive decade review and analysis on designs and performance parameters of passive solar still, Renewables Wind. Water, Sol (2015), https://doi.org/10.1186/s40807-015-0019-8.
[76] F.M. Abed, M.S. Kassim, M.R. Rahi, Performance improvement of a passive solar still in a water desalination, Int. J. Environ. Sci. Technol. (2017), https://doi.org/10.1007/s13762-016-1231-9.
[77] K.R. Ranjan, S.C. Kaushik, Exergy analysis of the active solar distillation systems integrated with solar ponds, Clean Technol. Environ. Policy (2014), https://doi.org/10.1007/s10098-013-0669-4.